BIROn - Birkbeck Institutional Research Online

Groom, Simon and Barfod, D.N. and Millar, I. and Downes, Hilary (2023) The Cumbre Nueva collapse (La Palma, Canary Islands): new age determinations and evidence of an isotopic excursion. Journal of Volcanology and Geothermal Research 433 (107708), ISSN 0377-0273.

Downloaded from: https://eprints.bbk.ac.uk/id/eprint/49629/

Usage Guidelines:
Please refer to usage guidelines at https://eprints.bbk.ac.uk/policies.html or alternatively contact lib-eprints@bbk.ac.uk.

THE CUMBRE NUEVA COLLAPSE (LA PALMA, CANARY ISLANDS): NEW AGE DETERMINATIONS AND EVIDENCE OF AN ISOTOPIC EXCURSION

Simon Groom[1], Dan N. Barfod[2], Ian Millar[3], Hilary Downes[1*]

[1] Dept. of Earth and Planetary Sciences, Birkbeck University of London, Malet Street, London WC1E 7HX UK
[2] National Environmental Isotope Facility, SUERC, East Kilbride G75 0QF UK
[3] National Environmental Isotope Facility, BGS, Keyworth NG12 5GG UK
* corresponding author

ABSTRACT

Episodic giant landslides characterize the history of intraplate oceanic volcanic islands, disrupting the gradual accumulation of eruptive products during shield-building stages. On La Palma (Canary Islands), the giant Cumbre Nueva collapse, which ended volcanic activity at the Paleo-Cumbre Nueva rift, formed the 11 km wide "Caldera de Taburiente" collapse embayment. Lavas erupted before and after this collapse have been studied, and $^{40}Ar/^{39}Ar$ ages of groundmass separates from key flows are presented, particularly from the small post-collapse Bejenado volcano that grew within the collapse scar. The new data constrain the age of the Cumbre Nueva collapse to between 519±20 ka and 529±12 ka (2σ) and confirm that it occurred during a period of rapid re-surfacing of the island. This study has also constrained the duration of activity of the post-collapse Bejenado volcano, and the results indicate that this was also brief (529±12 ka to 491±16 ka). Starting just before the time of the collapse, the radiogenic isotope compositions of the lavas shifted temporarily to more depleted compositions, perhaps indicating that an isotopically distinct magma source was being tapped. However, an isotopic excursion of similar magnitude also occurred later in the post-collapse activity, suggesting that the changes in isotope composition of the magma source continued during after the collapse.

Key words: volcano collapse, Ar-Ar dating, radiogenic isotopes

1. INTRODUCTION

Collapse of intraplate ocean island volcanoes has long been recognized as a major geological process (e.g., Moore et al., 1989; Day et al., 1999; Carracedo 1999; Masson et al., 2002; Hunt et al., 2013; Hunt and Jarvis., 2017; Blahut et al., 2018). Such collapses may be accompanied by changes in magma composition erupted before and after the event (Watt, 2019; Cornu et al., 2021). Understanding of the collapse history of volcanoes in the Canary Islands has advanced greatly over recent decades, including through many investigations of the submarine landslides they produced (Masson 1996; Marti et al., 1997; Carracedo et al.,1999a,b; Krastel et al., 2001; Hurliman et al. 2004; Leon et al., 2017). Geochronological studies have provided an absolute chronology for eruptive activity and collapse events (Thirlwall et al., 2000; Guillou et al., 2004a,b; Carracedo et al., 2007; Longpré et al., 2011). Here a revised history of the Cumbre Nueva collapse on La Palma (Guillou et al., 1998; 2001; Carracedo et al., 1999a,b, 2001) is presented, and changes in the radiogenic isotope composition of lavas erupted across the period of collapse and after it are discussed.

The Cumbre Nueva collapse occurred at "about 560 ka" (Carrecedo et al., 1999a, 2001), following a period of spatially focused volcanism along the Paleo-Cumbre Nueva rift zone. The post-collapse Bejenado volcanic edifice then grew within the collapse structure. The volcanism during this period, and the age of the Cumbre Nueva collapse, are the subjects of this high-resolution geochronological study. Previous geochronological studies (Carracedo et al., 2001; Guillou et al., 2001) yielded two key results: (1) pre-collapse Cumbre Nueva rift activity involved late rapid growth inferred to have occurred between 621±9 ka and 566±8 ka; (2) post-collapse activity was also the product of rapid growth, dated between 537±8 ka and 490±60 ka. The number of key events (volcano growth, volcano collapse, post-collapse volcano growth) in this brief period presents challenges to the sampling strategy and determination of radiometric dates.

To address these problems, stratigraphically well-constrained lava flow samples were collected from across the period of the Cumbre Nueva collapse, for which 13 new ages obtained by $^{40}Ar/^{39}Ar$ step-heating are presented. Sr, Nd and Pb radiogenic isotope studies of the lavas were also undertaken, to investigate any differences between the pre- and post-collapse magma reservoirs.

2. GEOLOGICAL CONTEXT OF SAMPLING

La Palma is one of the youngest and westernmost of the Canary Islands (Figure 1A). It is dominated by the older Taburiente shield volcano in the north, and the younger Cumbre Vieja ridge to the south (Figure 1B). These edifices are separated by a major unconformity, the product of the Cumbre Nueva collapse (Carracedo et al., 1999a,b). This collapse structure provides access to some of the island's oldest rocks and cliff sections through pre-collapse lava sequences. Subsequent incision of Barranco de las Angustias along the northern sidewall of the collapse has formed the spectacular erosional basin of the "Caldera de Taburiente" (Carracedo et al, 1999a; Paris and Carracedo, 2001; Colmenero et al., 2012). The cliffs of Caldera de Taburiente expose the most complete sections through the Taburiente shield volcano and the uplifted seamount rocks (Staudigel and Schminke, 1984) that underlie this region. Localities of lavas sampled and analysed in this study are shown in Figure 2.

Towards the end of volcanic activity of Taburiente, eruptions became focused in the south, forming the Paleo-Cumbre Nueva rift (Carracedo et al., 1999a; Navarro and Coello, 1994). This activity repeatedly re-surfaced the southern side of Taburiente volcano, with lavas from the Cumbre Nueva onlapping onto Taburiente rocks (Carracedo et al., 1999a; Day et al., 1999). There is no stratigraphic marker for the onset of this activity and it likely resulted from a gradual southward progression of volcanism (Carracedo et al., 1999a). However, Cumbre Nueva lavas are generally of normal magnetic polarity (Brunhes epoch), so the main period of growth occurred after 0.78 Ma, in contrast to Taburiente which contains mostly reverse-polarity Matuyama epoch rocks (Carracedo et al., 2001; Guillou et al., 1998, 2001).

The crest and much of the western side of the Paleo-Cumbre Nueva rift were removed by the collapse, but several authors (Carracedo et al., 1999b; Day et al., 1999; Navarro and Coello, 1994) have interpreted outcrops between the El Time cliff and Barranco Jurado as relics of its western flank. The constraints on the upper age limit for the collapse were obtained from surface lava flows in this area, while sections formed by fluvial incisions permitted access to older flows whose dates provide insights into pre-collapse re-surfacing rates. Barranco Jurado is incised along the northernmost outcrop of lavas erupted from the Paleo-Cumbre Nueva rift zone. The area between Barranco Jurado and the El Time cliff (the northern wall of Barranco de las Angustias) is the least eroded region of the Taburiente shield (Figure 2) where the topography of surface flows can often be followed up-flow until they are truncated to the east by Barranco de las Angustias. The truncated flows were the products of focused volcanism in the axial region of the Paleo-Cumbre Nueva rift. Thus, the cliff at Barranco de las Angustias has both preserved the lavas of this region from erosion and provided unambiguous evidence that these flows are the product of pre-collapse volcanism. This is important since previous studies have attributed any young dates from lava flows on Taburiente to post-collapse volcanism (Carracedo et al., 2001; Guillou et al., 2001), but in this area all lavas must predate the collapse.

Samples from El Time were collected from the deeply incised Barranco Jurado (referred to here as “unit 1”), from the smaller Barranco de los Gomeros (“unit 2”), and from roadcuts in surface flows (“unit 3”). These samples provide ages for the oldest accessible flows in the barrancos as well as surface flows that are some of the youngest preserved pre-collapse lavas. The pre-collapse samples are thus from a different region than those sampled and dated by Guillou et al (2001) and Carrecedo et al (2001). The El Time area has experienced much less erosion than the previously sampled section at Camino Ermita de la Peña on the Cumbre Nueva escarpment. In the El Time area, the interfluves between the barrancos retain lava flow channel and levee morphology, implying that the topmost pre-collapse lava flows are still in place, whereas the rest of the Taburiente volcano, including the Cumbre Nueva ridge, is deeply incised by V-shaped barrancos.

Lavas from El Time are mostly basanites and tephrites, dominated by phenocrysts of clinopyroxene and olivine, with some titanomagnetite, in a microlitic groundmass with sparse plagioclase. Clinopyroxenes are usually single complexly zoned phenocrysts, but can also occur as glomerocrysts. Euhedral augite rims often enclose sieve-textured or reverse-zoned green pyroxene cores. Crystal contents vary from sparsely porphyritic lavas with crystalline groundmasses dominated by plagioclase and clinopyroxene, to strongly porphyritic lavas which tend towards ankaramites. These contain up to 50% phenocrysts, largely consisting of single crystals of olivine and clinopyroxene that can be euhedral or fragmentary, and minor titanomagnetite. Their groundmasses contain small crystals of plagioclase, although one sample (LP12SG09) contains large (>4 mm) groundmass plagioclase laths. One sample from El Time (LP12SG22) is an amphibole phono-tephrite with phenocrysts of clinopyroxene, rounded kaersutitic amphibole rimmed by iron oxides, and titanomagnetite. Sodalite group minerals are also present as microphenocrysts. Clinopyroxene crystals often host inclusions of acicular apatite. Holocrystalline glomerocrysts composed of the same minerals are common. Groundmasses are plagioclase-rich, leading to trachytic textures.

2.2 Post-collapse rocks

Post-collapse samples were obtained from the Bejenado stratovolcano (Carrecedo et al., 2001). Deposits from Bejenado are exposed in cliffs of the Cumbre Nueva collapse scar on the southern side of “Caldera de Taburiente”. However, incision of “Caldera de Taburiente” has removed the summit of Bejenado as well as any direct contacts between Bejenado deposits and rocks of Taburiente volcano. This lack of exposed contacts between the Taburiente and Bejenado volcanoes adds to the importance of radiometric dating in determining the relationships between the two.

The oldest Bejenado sample (defined as “unit 4”) was collected from the Taburiente cliff. All other samples were taken from Bejenado’s southern flank which shows a marked distinction between its eastern and western parts (Figure 2). The west is deeply incised by canyons, while the east has a less well-developed drainage network, suggesting that the eastern lavas are younger. Some samples were obtained from west Bejenado (“unit 5”) but most of the samples are from east Bejenado (“unit 6” and “unit 7”). Unit 6 consists of tephrite lava flows intercalated with volcaniclastic sequences, whereas unit 7 is the overlying main effusive phase of Bejenado, consisting of a widespread basaltic flow field. Carracedo et al. (2001) used an increase in degree of evolution in magmatic composition towards the top of the sequence to distinguish the “Terminal Differentiated Vents” from the underlying main Bejenado stratovolcano. The steeply dipping southern flank of Bejenado is the primary remnant of the post-Cumbre Nueva collapse volcanism from which we sampled four surface flows (“unit 8” of this study) equivalent to the “Terminal Sheet Phase” of Carracedo et al. (2001). A lava from the parasitic cone Montana de la Hiedra (“unit 9”) was also sampled.

Primitive lavas from Bejenado are olivine- and clinopyroxene-phyric basanites with varying amounts of titanomagnetite phenocrysts. They have microlitic groundmasses containing small amounts of plagioclase. The ankaramites are largely glomeroporphyritic, rich in aggregates of the same minerals that are present as phenocrysts. Some Bejenado lavas are more evolved than those of El Time, but in contrast to El Time lavas, amphibole is largely absent except in the phono-tephrites. They also contain zoned sodalite-group minerals (nosean cores and blue hayune rims).

3. METHODS

Samples were collected in the field on grounds of freshness, and screened prior to crushing. Aliquots of 34 representative samples were powdered and analysed for bulk geochemistry by XRF at Royal Holloway University of London. Results are reported in Table 1, and data presented in Figures 3-5.

For Ar-Ar dating, two 300 mg aliquots of separated groundmass material (250-500 μm fraction) were prepared by jaw-crushing and sieving. Alteration-free groundmass separates were then purified by a combination of leaching in dilute HNO_3, magnetic separation, and meticulous hand-picking under a binocular microscope. Hand-picking focused on the removal of any remaining phenocrysts and grains with evidence of alteration. Dated samples were mostly of basanite to tephrite composition, with a phono-tephrite sample showing the most evolved composition (see Table 1 for whole rock XRF analyses). However, the strongly porphyritic ankaramites present in both the pre-collapse and post-collapse suites presented a risk of argon inheritance, and these samples were therefore subject to the most rigorous preparation procedures of the sample suite. Furthermore, a few samples were found to contain small xenoliths, which were removed during sample preparation.

Preparation and analysis followed the protocols established at the NEIF Argon Isotope Laboratory at SUERC in East Kilbride. Samples and neutron flux monitors were placed in copper foil packets and stacked in quartz tubes. The relative positions of the packets were precisely measured for later reconstruction of neutron flux gradients.

The sample package was irradiated for 2 hours in the Oregon State University reactor, Cd-shielded facility. Alder Creek sanidine (1.1891 ± 0.0008 (1σ) Ma (Niespolo et al., 2017) was used to monitor ^{39}Ar production and establish neutron flux values for the samples.

Gas was extracted from samples via step-heating using a mid-infrared (10.6 μm) CO_2 laser, with samples housed in a doubly pumped ZnS-window laser cell. Individual sample grains (either 50 mg or 120 mg) were loaded into a copper planchette containing 1.0 x 1.0 cm square wells. Liberated argon was then purified of active gases (e.g., CO_2, H_2O, H_2, N_2, CH_4) using three Zr-Al getters; one at 16°C and two at 400°C. Data were collected on a GVi instruments ARGUS V multi-collector mass spectrometer using a variable sensitivity faraday collector array in static collection mode (Sparks et al., 2008; Mark et al., 2009). Time-intensity data were regressed to t_0 with second-order polynomial fits to the data. Mass discrimination was monitored by comparison to running-average values of an air standard. The average total system blank, measured between each sample run, was 2 x 10^{-15} mol ^{40}Ar, 9 x 10^{-17} mol ^{39}Ar and 3 x 10^{-17} mol ^{36}Ar.

All data were corrected for blanks, interference and mass discrimination using the Massspec software package (authored by Al Deino, BGC, Version 8.058). Decay constants and corrections after Renne et al. 2011 (see Supplementary Tables). Steps with ≤ 1% ^{39}Ar yield were rejected from plateau calculations. Plateau acceptance criteria were that the plateau consists of at least five contiguous steps and that these steps are indistinguishable at 2σ uncertainty. Scatter between the ages of the steps is low, i.e., MSWD close to 1, and the fraction of ^{39}Ar released for these steps is ≥50%. Isochrons were calculated using only the plateau steps to determine the composition of the trapped component. A plateau age was accepted if it was concordant at the 2σ level with the isochron age, had a trapped component indistinguishable from air (298.56±0.31, 1σ) at the 2σ level and met the other criteria listed above. Replicated samples, for example LP12SG87, were combined using the accepted steps from two experiments to produce a composite plateau and isochron. Where available, composite plateaux are accepted as the best estimate of the eruption age. Examples are shown in the Figure 6, and results are presented in Table 2.

Whole rock isotope analyses were conducted at the National Environmental Isotope Facility in Keyworth. Approximately 250 mg of powdered sample were weighed precisely into Savillex beakers and leached on a hotplate in 6M HCl at 60°C for 30 minutes, prior to dissolution in a mixture of HF and HNO_3. They were converted to nitrate or chloride form, as appropriate. Sr and Pb were separated using SR-SPEC ion exchange resin following the methods of Deniel and Pin (2001). Nd was separated using a primary cation exchange column (Eichrom AG-50), followed by a LN-SPEC column. Procedural blanks for Sr, Nd and Pb during the time of analysis were <100 pg.

Sr fractions were loaded onto outgassed single Re filaments using a TaO activator solution, and analysed in multi-dynamic mode on a Thermo Scientific Triton mass spectrometer. Data were normalised to $^{86}Sr/^{88}Sr$ = 0.1194. Fifty-five measurements of the SRM987 Sr standard run during the time of sample analysis gave a value of $^{87}Sr/^{86}Sr$ of 0.710254±6 (1 sigma). Nd fractions were loaded onto one side of an outgassed double Re filament assembly using dilute HCl, and analysed in multi-dynamic mode on the same Triton instrument. Data were normalised to $^{146}Nd/^{144}Nd$ = 0.7219. Twenty analyses of the JND-I standard gave a value of 0.512098±11. All data are quoted relative to a value of 0.512115 for this standard. Prior to Pb isotope analysis, each sample was spiked with a Tl solution, added to allow for correction of instrument-induced mass bias. Samples were introduced into the NU instruments NU plasma MC-ICP-MS, using an ESI 50µl/min PFA micro-concentric nebuliser. The accuracy and precision of the method was assessed by repeated analysis of a Tl-doped NBS 981 Pb reference standard and comparison with the known values of this reference material (Thirlwall 2002). Results presented in Table 3.

4. RESULTS

4.1 BULK ROCK GEOCHEMISTRY

The analysed samples are fresh with almost all having Loss on Ignition (LOI) values below 0.5 wt% (Table 1) and many LOI values are negative (i.e., the sample gained on ignition because of oxidation of FeO). Pre-and post-collapse lavas from La Palma cover the range of alkaline rocks from basanite to tephri-phonolite (Figure 3). The two suites of lavas overlap compositionally in this diagram, although those from Bejenado extend to more fractionated compositions than those from El Time. The same is seen in “Harker”-style diagrams of major element oxides vs MgO (Figure 4A), where MgO is used as a fractionation index in preference to SiO_2, because SiO_2 does not vary during the first stage of fractionation (from 16 to 4 wt% MgO). One El Time sample has a substantially higher MgO content than all others, which may be related to accumulative olivine. Points of inflection at 6 wt % MgO are seen for CaO, Fe_2O_3 and TiO_2, indicating a change in mineral extract, probably the end of olivine fractionation. A second point of inflection at 4 wt% MgO is clear from the diagram for P_2O_5, resulting from the onset of apatite fractionation. Two post-collapse samples have unusually high P_2O_5 contents that may relate to the presence of apatite inclusions in clinopyroxene phenocrysts.

The main fractionating phases that caused the variations in major and trace element compositions are olivine, clinopyroxene, titanomagnetite and apatite. Disappearance of olivine from the mineral extract is the main cause of the infection point at 6 wt% MgO, and the start of apatite fractionation caused the second inflection point at 4 wt% MgO. This is in agreement with the conclusions of Day et al. (2010), who modelled these processes in more detail. The main point to be made about the major element geochemistry is that, apart from the greater degree of fractionation in the post-collapse lavas, there is no difference between the lavas erupted before or after the Cumbre Nueva collapse. A single high-MgO lava (sample LP13SG06) is also present in the pre-collapse sequence.

Trace elements in the two groups of lavas also show almost no difference in composition (Figure 4B), although the high-MgO lava from El Time shows an unusually high Sc content. However, its Ni content is identical to that of post-collapse lavas with significantly lower MgO (13 wt% MgO). On mantle-normalised trace element diagrams (Figure 5), the pre- and post-collapse lavas show identical patterns, closely resembling those given by Day et al. (2010) for pre-collapse Taburiente lavas. Once again, sample LP13SG06 is anomalous in that it has the lowest abundances of incompatible trace elements (except Rb) in all analysed samples. The geochemistry of this sample can be best explained as that of a typical La Palma alkali basalt/basanite that has accumulated clinopyroxene in agreement with its clinopyroxene-rich appearance in hand specimen and thin section (i.e., it is ankaramitic). Those lavas previously identified as having high P_2O_5 also show unusually high abundances of trace elements such as Sr and Y.

4.2 GEOCHRONOLOGY AND ISOTOPE RESULTS

Localities for samples of dated lava flows are shown in Figure 2, with ages given in Table 2. Representative Ar-Ar data are shown in Figure 6 and the locations of the samples in the regional stratigraphy in Figure 7. Plateau ages passed the verification criteria except for LP14SG02 (discussed below), and therefore plateau ages provide the most precise estimate of emplacement date. The 2σ errors are all 1.2-5.5% relative.

The age of the stratigraphically lowermost El Time pre-collapse sample (LP13SG05) is 604±7 ka. The short interval until eruption of an up-sequence flow in Barranco Jurado (LP13SG06, 574±11 ka) suggests rapid re-surfacing. This is supported by the stratigraphically lowest flow sampled from Barranco de los Gomeros (LP12SG15) (541±30 ka). Activity continued until the eruption of the LP12SG14 and LP12SG10 lava flows, which are among the Paleo-Cumbre Nueva rift's youngest extant products. An age of 529±12 ka for LP12SG14 provides the best radiometric date for the end of the pre-collapse volcanic activity at El Time.

Samples from the lower part of the post-collapse Bejenado volcano (units 4-6) all yield dates between 505 and 523 ka (Table 2), with the exception of LP14SG02 which gives an older age, inconsistent with its stratigraphic location. The non-atmospheric intercept of its isochron indicates inherited Ar, and the presence of xenolithic material in this flow supports this interpretation. This sample was therefore disregarded from further interpretation. Lavas from higher in the Bejenado sequence yield ages as young as 490±17 ka. The new data may indicate that the samples form distinct older (units 4, 5, 6) and younger (unit 7, 8) groups, with the exception of sample LP13SG29. However, the latter is from an area where the boundary between unit 6 and unit 7 is not well constrained, and its ankaramitic composition is closer to rocks in the older units than to the more evolved rocks in the younger units.

Sample LP14SG07 from Montaña de la Hiedra yields an age for the latest Bejenado eruptions at 491±16 ka, in contrast to the previous age determination of 580±30 ka (Guillou et al. 2001). However, LP14SG07 is from near the top of Montaña de la Hiedra whereas the previous sample was from a barranco on its eastern flank. Thus, the latter may be an inadvertent sample of an older unit mostly covered by the Montana de la Hiedra activity.

The co-variation of Sr-Nd isotope compositions for 34 lavas from La Palma (12 from El Time; 20 from Bejenado; 2 from Montana de la Hiedra) is shown in Figure 8. As seen in earlier studies (Figure 8), samples from El Time (pre-collapse) and samples from Bejenado (post-collapse) overlap to a great extent, although the post-collapse ones tend to show more depleted isotope compositions.

The radiogenic isotope data, ordered in the inferred stratigraphic succession, are displayed in Figure 9. There are no significant differences between pre-collapse and post-collapse lavas in the total variation of Sr, Nd or Pb isotopes, except the oldest post-collapse sample (LP13SG38) that has a much lower ^{87}Sr/^{86}Sr and all Pb isotope ratios, and a higher ^{143}Nd/^{144}Nd value. One of the uppermost pre-collapse samples (LP12SG18) is similar, having the highest ^{143}Nd/^{144}Nd value of all analyzed samples, together with low ^{207}Pb/^{204}Pb and ^{208}Pb/^{204}Pb values. However, samples with similar depleted isotope compositions also occur in unit 7, in lavas erupted after the collapse.

5. DISCUSSION

5.1 Age of the Cumbre Nueva collapse

The results of this study (Table 1) provide ages of 529±12 ka for the youngest dated pre-collapse eruption, and 519±20 ka for the earliest post-collapse eruption. Thus, the date the Cumbre Nueva collapse has been determined to be ≈525 ka, supported by ages from stratigraphically younger or older flows (Figure 7). The date obtained in the present work is somewhat younger than the previous estimate of ≈560 ka (Carracedo et al., 2001; Guillou et al., 2001, 1998). Those studies used a date from the significantly more altered flows of the Cumbre Nueva ridge to provide the pre-collapse bracket and interpreted their six younger ages from the Taburiente edifice as post-collapse volcanism. However, the topmost lavas preserved at the Cumbre Nueva ridge are severely altered and were not dated by the previous studies. The topmost sample in Carracedo et al. (2001) was collected at 1400 m asl, whereas the crest of the ridge is at 1425 m asl. Because the previous work was carried out in conjunction with palaeomagnetic studies, their sample sites can be identified by drill holes, and we found the topmost holes at ~25 m below the top of the section. It is therefore likely that their youngest pre-collapse sample was covered by two or more younger flows before the Cumbre Nueva collapse, representing a time interval of some 10s of thousands of years, assuming a resurfacing rate similar to that in the younger Cumbre Vieja volcano (Guillou et al., 1998).

This new dating helps to resolve the question of whether volcanic activity continued on the Taburiente volcano after the Cumbre Nueva collapse, while Bejenado grew within the collapse scar, as proposed by Carracedo et al. (2001). It is plausible that such activity could have continued, as seen on other ocean island volcanoes, such as Fogo (Cape Verdes) with the rapid growth of the Pico do Fogo edifice (~ 2 km thick sequence) at the same time as a few tens of metres of lavas erupted on the flank from vents outside the collapse scar (Foeken et al., 2009). However, on the basis of the younger estimate for the collapse from this study, only two of the previous 32 age determinations from Taburiente reported by Carracedo et al. (2001) and Guillou et al. (2001) would be consistent with post-collapse volcanism.

The younger date for the Cumbre Nueva collapse also has implications for the correlation with offshore turbidites. Hunt et al. (2013) favored a date of 480-490 ka for the turbidite that they correlated with the Cumbre Nueva collapse, so the younger age determined here might reduce the discrepancy between onshore and offshore evidence. However, based on the chronology presented here, a prediction can be made that any widespread turbidite unit that might have been produced by the Cumbre Nueva collapse would be found in Madeira abyssal plain deposits of around 525 ka old. A number of turbidite beds with such ages were identified by Hunt et al. (2013) but were ascribed to collapses of other Canary Island edifices. Material from the Cumbre Nueva collapse may be found within that group of turbidites.

All the studied lava flows yielded ages between 604±7 ka and 491±16 ka. The ≈70 ka period prior to the Cumbre Nueva collapse saw emplacement of successions of flow-fields in the El Time area, consistent with the conclusion of Carracedo et al. (1999a,b, 2001) that the Cumbre Nueva segment of the Taburiente edifice was constructed in a brief period. An approximate re-surfacing rate can be estimated for this area of one flow every 20 ka. Thus, rates over this period are generally similar to those observed in recent activity at the Cumbre Vieja to the south (Carracedo et al., 2001).

Post-collapse volcanism at Bejenado occurred from 523±11 ka to 491±16 ka, indicating that this was also the product of a brief period of rapid and focused volcanism. Bejenado is a small edifice because it was short-lived, although with a high eruption rate. However, it is difficult to determine quite how brief its activity was, because the variation in age estimates from stratigraphically young and old flows is of a similar magnitude to individual analytical uncertainties. Nevertheless, the implication is that the rapid but brief growth of Bejenado, together with the good sections created by erosion, make it an excellent site in which to study volcanism in the immediate aftermath of a giant lateral collapse.

5.2 Sr-Nd isotope variations

Isotope data for the analyzed samples (Figure 8) are similar to previously published range for La Palma which are considered to be the product of mixtures of HIMU (High U/Pb) and Depleted MORB-Source mantle (DMM) components (Gallipp, 2005; Praegel and Holm, 2005; Gurenko et al., 2006; Day et al., 2010). The only difference between the pre- and post-collapse lavas is that the post-collapse lavas tend to show more isotopically depleted compositions (i.e., closer to the DMM component). This could imply that a previously untapped, more isotopically depleted, mantle reservoir became able to supply magma after the collapse event. This component is similar to (but slightly more depleted than) that which supplied the most depleted isotopic compositions seen in La Palma (Figure 8). A similar isotopic excursion to more depleted compositions after a major collapse on Fogo in the Cape Verde archipelago has been reported by Cornu et al. (2021).

The lava flow erupted immediately after the Cumbre Nueva collapse (LP13SG38) shows a significant shift to values closer to the DMM component (i.e., low $^{87}Sr/^{86}Sr$, high $^{143}Nd/^{144}Nd$ and low radiogenic Pb isotope compositions) (Figure 9). These features are shared in part by one of the youngest pre-collapse lava flows (LP12SG18), although this sample does not have a low $^{87}Sr/^{86}Sr$ ratio. This isotopic excursion confirms that a different mantle source was tapped or that a pocket of magma derived from such a source was able to erupt at this time. This change in the magmatic source across a volcanic collapse could support the observations of Watt (2019) that erupted magma compositions often change before or during a collapse. It may relate to structural changes in the volcano and, in particular, the release of pressure on the magma reservoir system. However, the change in isotope composition of erupted lavas that occurred at the collapse was repeated later in the stratigraphy (Figure 9), as an identical isotopic excursion occurred between units 6 and 7. This implies that, although the change in isotope composition that occurred around the time of the collapse might have been related to the structural changes in the volcano, the new batch of magma continued to be tapped long after the collapse occurred.

6. CONCLUSIONS

A revised age for the Cumbre Nueva collapse on La Palma has been determined as ca. 525 ka, using a new sampling strategy and high precision Ar-Ar step-heating. An age of 491±16 ka is also provided for the Montana de la Hiedra parasitic cone that is more consistent with its volcanic setting (i.e., from field relations, it appears to overlie the Bejenado volcanic deposits, so a younger age is to be expected).

This study has shown that there is little difference in bulk major and trace element compositions between lavas erupted before and after the Cumbre Nueva collapse, although the upper lavas from the post-collapse Bejenado volcano tend to be more evolved. This may be related to tapping of fractionated magma reservoirs trapped in the volcanic edifice.

The isotope results presented here show that there are no differences between pre- and post-collapse lavas, but that a major isotopic change occurred in the erupted products around the time of the collapse. However, a very similar change is also observed in isotope data within the post-collapse sequence, so this isotopic excursion may not be linked to structural changes in the island due to the onset of volcano collapse.

ACKNOWLEDGEMENTS

We acknowledge a NEIF Argon Isotope grant (NEIFSC 1355-1112) and NERC isotope grant IP-1477-1114. This study was supported by Birkbeck and the Geological Society of London. Staff at Royal Holloway University of London are thanked for access to X-Ray

Fluorescence. We are grateful to two anonymous reviewers whose comments greatly improved the manuscript.

Tables

Unit number	9	9	8	8	8
Location	La Hiedra	La Hiedra	Bejenado	Bejenado	Bejenado
Sample	**LP14SG07**	LP13SG34	LP13SG28	LP13SG10	LP13SG13
UTM co-ordinates	219093/317420	219589/317468	220585/317616	215226/317580	219255/317619
SiO_2	43.66	43.28	47.40	40.22	48.05
Al_2O_3	15.17	14.80	18.24	13.63	18.03
Fe_2O_3	12.44	12.23	8.77	14.87	8.33
MgO	4.06	3.86	3.30	7.22	2.21
CaO	10.00	9.80	7.43	11.99	6.70
Na_2O	5.99	6.19	6.60	3.62	7.80
K_2O	2.80	2.78	3.16	1.18	3.58
TiO_2	3.67	3.57	2.66	4.08	2.55
MnO	0.27	0.26	0.18	0.22	0.21
P_2O_5	1.28	1.23	0.74	1.03	0.59
Total	100.27	98.86	99.20	99.39	99.00
LOI	0.11	0.60	0.61	0.56	0.49
Ni	11	11	23	71	7
Cr	10	12	25	98	4
V	245	230	210	379	171
Sc	10	9	7	23	3
Cu	37	35	35	85	20
Zn	147	149	103	123	129
Ga	29.9	29.4	27.9	20.8	31.3
Pb	8.2	7.9	8.0	3.5	10.7
Sr	1585.9	1631.0	1441.5	968.9	1602.7
Rb	81.6	81.8	82.2	40.3	109.6
Ba	954.3	904.8	917.1	569.2	993.9
Zr	837.4	839.8	635.1	328.3	884.2
Nb	201.3	200.7	182.9	101.4	214.3
Ta	12.6	13.2	10.7	5.9	12.4
Th	10.7	10.6	12.4	6.3	13.3
U	2.5	2.4	3.3	1.4	3.4
Y	43.0	43.6	31.4	33.6	37.4
La	109.8	107.9	89.0	74.3	106.2
Ce	213.3	217.4	161.4	142.0	196.4
Nd	99.9	101.7	64.2	66.9	80.4
Sm	17.8	17.1	10.6	12.5	11.7

Table 1. Grid reference and XRF analyses of La Palma samples analyzed in this study. Composition of standard BCR-2 is also shown EXAMPLES ONLY – PLEASE ASK CORRESPONDING AUTHOR FOR FULL DOCUMENT

Sample	Material	Plateau Age (Ma)	± 2s w/o J	± 2s w/J	MSWD	p	n/n-tot	%gas
LP12SG87_1	Groundmass	0.541	0.040	0.040	0.70	0.69	9/9	100
LP12SG87_2	Groundmass	0.520	0.012	0.013	0.80	0.57	9/9	100
all plat. steps	Groundmass	**0.523**	**0.011**	0.012	0.80	0.70	18/18	100
LP13SG06_1	Groundmass	0.544	0.05	0.050	0.70	0.81	14/14	100
LP13SG06_2	Groundmass	0.576	0.011	0.012	1.20	0.29	10/12	95.7
all plat. steps	Groundmass	**0.574**	**0.011**	0.012	0.90	0.58	24/24	100
LP13SG05_1	Groundmass	0.596	0.020	0.020	1.60	0.11	10/14	88.8
LP13SG05_2	Groundmass	0.605	0.007	0.009	1.90	0.06	9/11	91.7
all plat. steps	Groundmass	**0.604**	**0.007**	0.009	1.70	0.04	19/19	100
LP13SG16	Groundmass	**0.500**	**0.014**	0.015	1.50	0.10	14/14	100
LP13SG29	Groundmass	**0.525**	**0.020**	0.020	0.70	0.74	14/14	100
LP13SG30	Groundmass	**0.505**	**0.016**	0.017	1.20	0.27	13/13	100
LP13SG38_1	Groundmass	0.543	0.050	0.050	0.60	0.83	14/14	100
LP13SG38_2	Groundmass	0.515	0.020	0.020	0.60	0.78	10/10	100
all plat. steps	Groundmass	**0.519**	**0.020**	0.020	0.60	0.90	24/24	100
LP14SG02	Groundmass	0.727	0.050	0.050	1.30	0.24	7/14	56.8
LP14SG02*	Groundmass	0.577	0.060	0.060	0.40	0.87	7/7	100
LP14SG07	Groundmass	**0.491**	**0.016**	0.017	0.70	0.78	13/13	100
LP14SG09	Groundmass	0.492	0.017	0.019	0.50	0.91	12/14	93.6
LP14SG09-F	Plagioclase	0.430	0.110	0.110	0.50	0.82	7/7	100
LP14SG09, and -F; all plat. steps	Plagioclase, Groundmass	**0.490**	**0.017**	0.019	0.50	0.95	19/19	100
LP12SG02	Groundmass	**0.509**	**0.011**	0.011	0.70	0.63	6/8	83
LP12SG10_1	Groundmass	0.544	0.030	0.030	1.10	0.34	8/8	100
LP12SG10_2	Groundmass	0.553	0.018	0.019	1.80	0.10	7/8	83.6
all plat. steps	Groundmass	**0.550**	**0.015**	0.017	1.40	0.17	15/15	100
LP12SG14_1	Groundmass	0.541	0.016	0.018	0.50	0.80	7/8	93.3
LP12SG14_2	Groundmass	0.516	0.018	0.019	2.20	0.06	6/8	88.3
all plat. steps	Groundmass	**0.529**	**0.012**	0.014	1.50	0.11	13/13	100
LP12SG15_1	Groundmass	**0.541**	**0.030**	0.030	1.00	0.41	8/8	100

Table 2. Ar-Ar geochronological data for all samples analyzed in this study. Full data can be found in the Supplementary Table. EXAMPLES ONLY – PLEASE ASK CORRESPONDING AUTHOR FOR FULL DOCUMENT

Eruption order	Location	Sample	87Sr/86Sr	± 2SE	143Nd/144Nd	± 2SE
9	Montana la Hiedra	**LP14SG07**	0.703139	0.000009	0.512869	0.000009
9	Montana la Hiedra	LP13SG34	0.703133	0.000005	0.512908	0.000006
8	East Bejenado	LP13SG28	0.703090	0.000010	0.512909	0.000009
8	East Bejenado	LP13SG10	0.703098	0.000004	0.512907	0.000005
8	East Bejenado	LP13SG13	0.703144	0.000005	0.512902	0.000007
8	East Bejenado	**LP13SG16**	0.703137	0.000003	0.512897	0.000005
8	East Bejenado	LP14SG10	0.703047	0.000005	0.512945	0.000004
7	East Bejenado	**LP13SG29**	0.702994	0.000010	0.512980	0.000008
7	East Bejenado	LP14SG04	0.703046	0.000007	0.512908	0.000009
7	East Bejenado	LP14SG05	0.703052	0.000011	0.512914	0.000008
7	East Bejenado	LP14SG06	0.703033	0.000009	0.512938	0.000008
7	East Bejenado	LP14SG08	0.702969	0.000010	0.512979	0.000006
7	East Bejenado	**LP14SG09**	0.703009	0.000008	0.512941	0.000009
7	East Bejenado	LP12SG03	0.702998	0.000006	0.512969	0.000009
7	East Bejenado	LP12SG05	0.703027	0.000004	0.512979	0.000013
7	East Bejenado	LP12SG82	0.703012	0.000007	0.512952	0.000007
6	East Bejenado	**LP13SG30**	0.703097	0.000025	0.512882	0.000007
6	East Bejenado	LP13SG26	0.703074	0.000004	0.512896	0.000008
5	West Bejenado	**LP12SG87**	0.703064	0.000006	0.512923	0.000007
5	West Bejenado	LP13SG01	0.703122	0.000005	0.512911	0.000007
5	West Bejenado	LP13SG11	0.703143	0.000007	0.512908	0.000007
4	Basal Bejenado	**LP13SG38**	0.702973	0.000010	0.512982	0.000013
3	El Time surface flows	LP12SG22	0.703028	0.000014	0.512925	0.000009
3	El Time surface flows	**LP12SG10**	0.703076	0.000008	0.512915	0.000009
3	El Time surface flows	**LP12SG14**	0.703075	0.000008	0.512906	0.000015
3	El Time surface flows	LP12SG23	0.703066	0.000008	0.512908	0.000009
3	El Time surface flows	LP12SG26	0.703081	0.000008	0.512897	0.000009
3	El Time surface flows	LP12SG09	0.703105	0.000007	0.512894	0.000013
3	El Time surface flows	LP12SG18	0.703060	0.000010	0.513001	0.000010
2	Barr. de los Gomeros	**LP12SG15**	0.703083	0.000007	0.512882	0.000010
1	Barranco Jurado	**LP13SG05**	0.702988	0.000007	0.512924	0.000008
1	Barranco Jurado	**LP13SG06**	0.703055	0.000010	0.512906	0.000010
1	Barranco Jurado	LP13SG32	0.703128	0.000005	0.512918	0.000007
1	Barranco Jurado	LP13SG07	0.703104	0.000005	0.512904	0.000007

Sample	$^{206}Pb/^{204}Pb$	± 2σ	$^{207}Pb/^{204}Pb$	± 2σ	$^{208}Pb/^{204}Pb$	± 2σ
LP14SG07	19.8184	0.0021	15.6234	0.0019	39.7291	0.0053
LP13SG34	19.8299	0.0023	15.6273	0.0024	39.7486	0.0068
LP13SG28	19.6239	0.0019	15.6099	0.0018	39.4710	0.0051
LP13SG10	19.8694	0.0024	15.6319	0.0024	39.7470	0.0070
LP13SG13	19.8266	0.0023	15.6255	0.0023	39.7326	0.0067
LP13SG16	19.8287	0.0023	15.6263	0.0023	39.7379	0.0068
LP14SG10	19.5094	0.0023	15.5997	0.0023	39.3345	0.0067

LP13SG29	19.1616	0.0021	15.5686	0.0020	38.9120	0.0056
LP14SG04	19.5325	0.0020	15.6001	0.0019	39.3586	0.0053
LP14SG05	19.5173	0.0019	15.6024	0.0018	39.3513	0.0052
LP14SG06	19.4199	0.0020	15.5898	0.0019	39.2209	0.0052
LP14SG08	19.1755	0.0021	15.5686	0.0020	38.9229	0.0055
LP14SG09	19.4212	0.0022	15.5905	0.0020	39.2253	0.0055
LP12SG03	19.1699	0.0023	15.5694	0.0024	38.9124	0.0067
LP12SG05	19.1586	0.0023	15.5652	0.0024	38.8925	0.0067
LP12SG82	19.1903	0.0023	15.5737	0.0024	38.9510	0.0068
LP13SG30	19.7820	0.0020	15.6187	0.0019	39.6731	0.0052
LP13SG26	19.8371	0.0025	15.6259	0.0024	39.7250	0.0070
LP12SG87	19.7539	0.0024	15.6256	0.0024	39.6098	0.0068
LP13SG01	19.8898	0.0026	15.6345	0.0025	39.7313	0.0072
LP13SG11	19.7655	0.0024	15.6237	0.0024	39.6188	0.0069
LP13SG38	19.0861	0.0020	15.5638	0.0020	38.8095	0.0053
LP12SG22	19.4593	0.0022	15.5962	0.0020	39.2469	0.0056
LP12SG10	19.6763	0.0021	15.6032	0.0020	39.5099	0.0054
LP12SG14	19.7131	0.0022	15.6159	0.0020	39.4908	0.0055
LP12SG23	19.8828	0.0022	15.6351	0.0020	39.7271	0.0055
LP12SG26	19.7051	0.0022	15.6124	0.0020	39.6259	0.0054
LP12SG09	19.7085	0.0023	15.6122	0.0024	39.6443	0.0069
LP12SG18	19.1091	0.0026	15.5669	0.0025	38.8350	0.0071
LP12SG15	19.8773	0.0024	15.6380	0.0021	39.7093	0.0060
LP13SG05	19.3306	0.0021	15.5843	0.0020	39.0869	0.0054
LP13SG06	19.8071	0.0027	15.6220	0.0024	39.6730	0.0066
LP13SG32	19.9788	0.0025	15.6496	0.0024	39.8261	0.0069
LP13SG07	19.6929	0.0025	15.6097	0.0024	39.6046	0.0070

Table 3. Sr and Nd isotope compositions of analyzed samples, in stratigraphic order (oldest at bottom).

Figures and Figure Captions

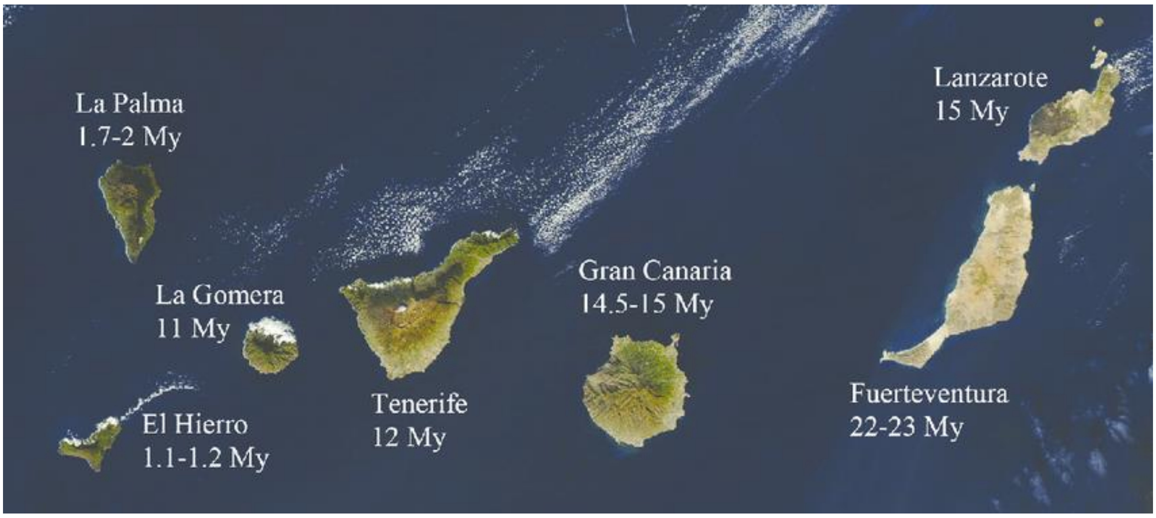

498 Figure 1A. Map of Canary Islands, showing location of La Palma as one of the youngest
499 and westernmost islands. Ages after Carrecedo et al. (1998) and van den Bogaard (2013).

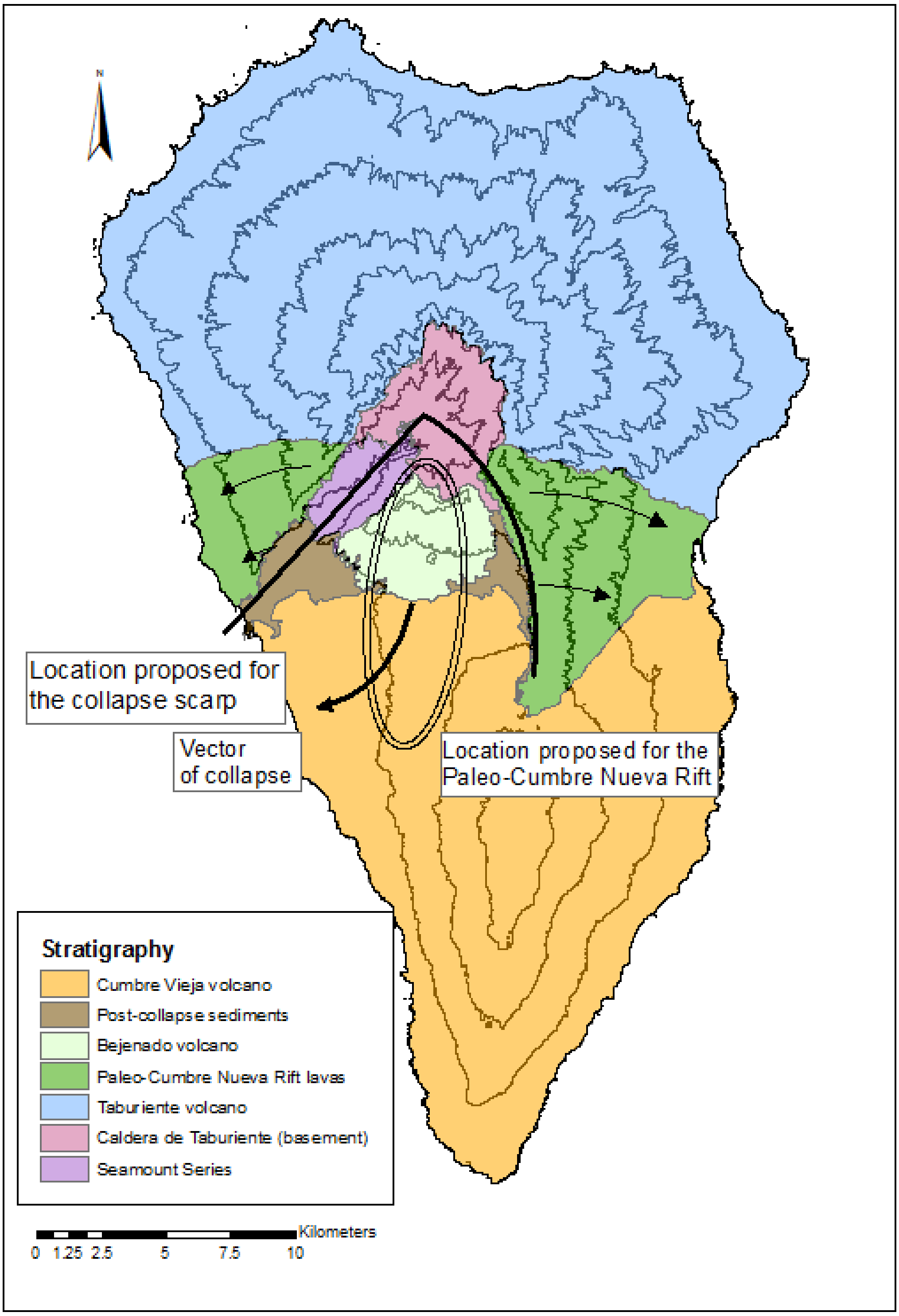

500

Figure 1B. Simplified topographic and geological map of La Palma, based on maps by Navarro and Coello 1994; Carracedo et al., 1999a; Day et al., 1999. Broad single arrow indicates direction of Cumbre Nueva collapse. Narrow arrows indicate direction of pre-collapse Cumbre Nueva rift lava flows. Samples in this study come from the Paleo-Cumbre Nueva Rift lavas (units 1 to 3) and the post-collapse Bejenado volcano (units 4 to 9).

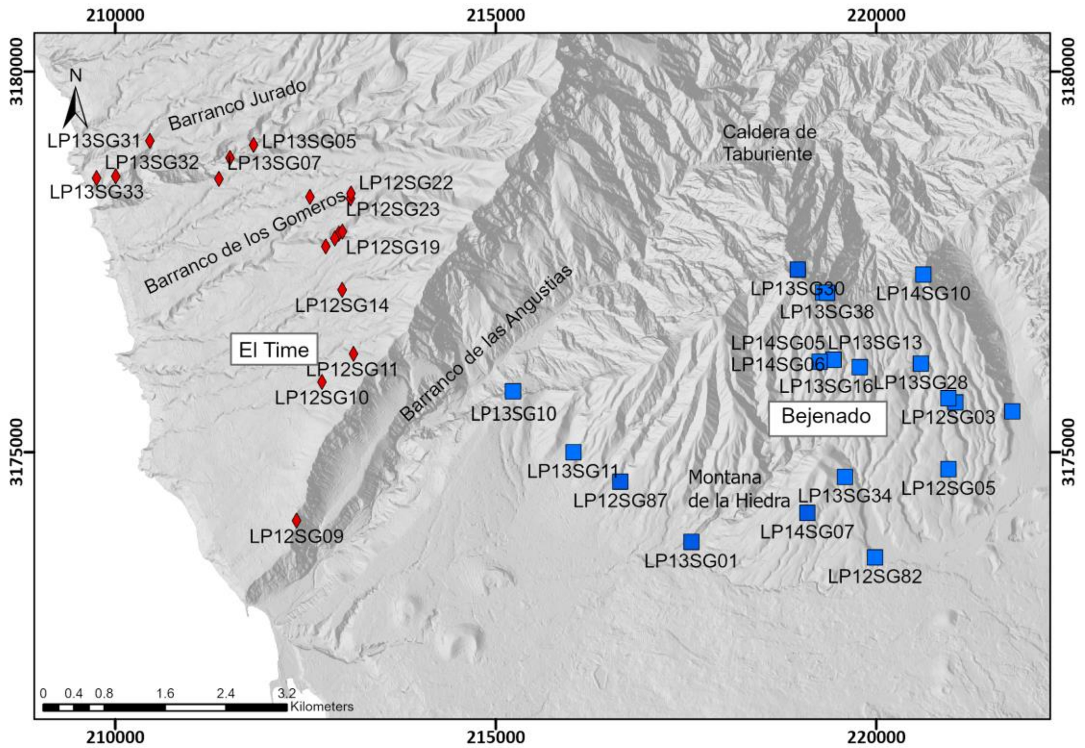

Figure. 2. Topographic image of central La Palma showing localities of lavas analysed in this study. Pre-collapse sample localities are shown in red; post collapse sample localities are shown in blue.

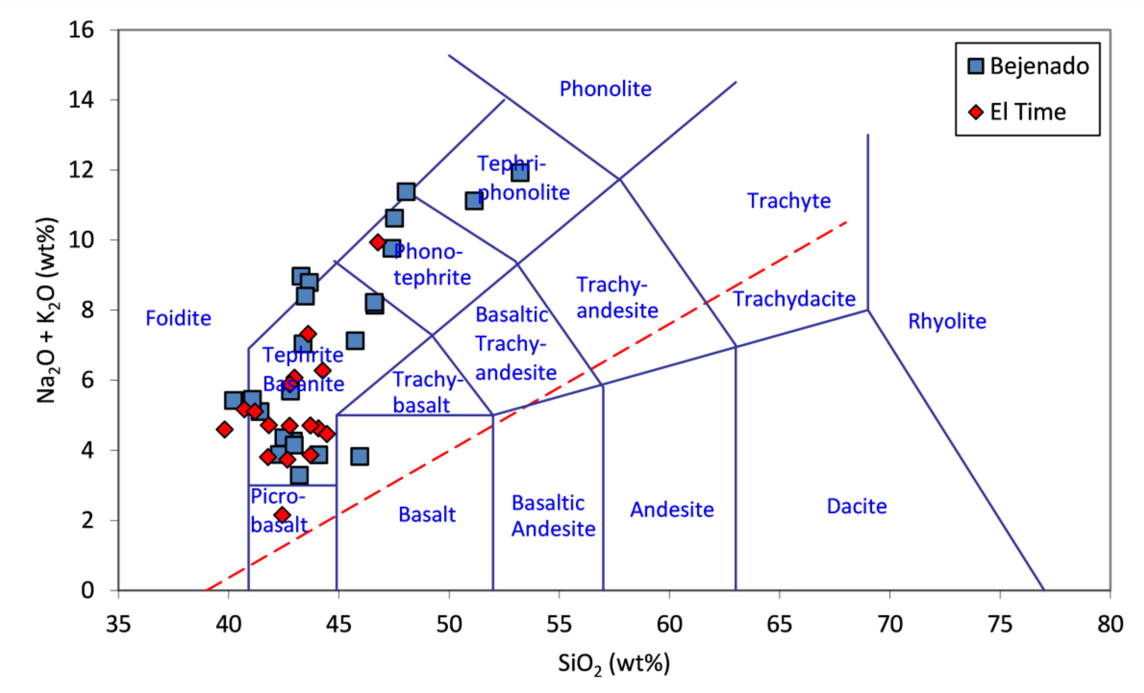

Figure 3. Total Alkali vs Silica (TAS) diagram for pre- and post-collapse lavas from La Palma. Pre-collapse samples from El Time are shown as solid symbols; post-collapse lavas from Bejenado are shown as open symbols.

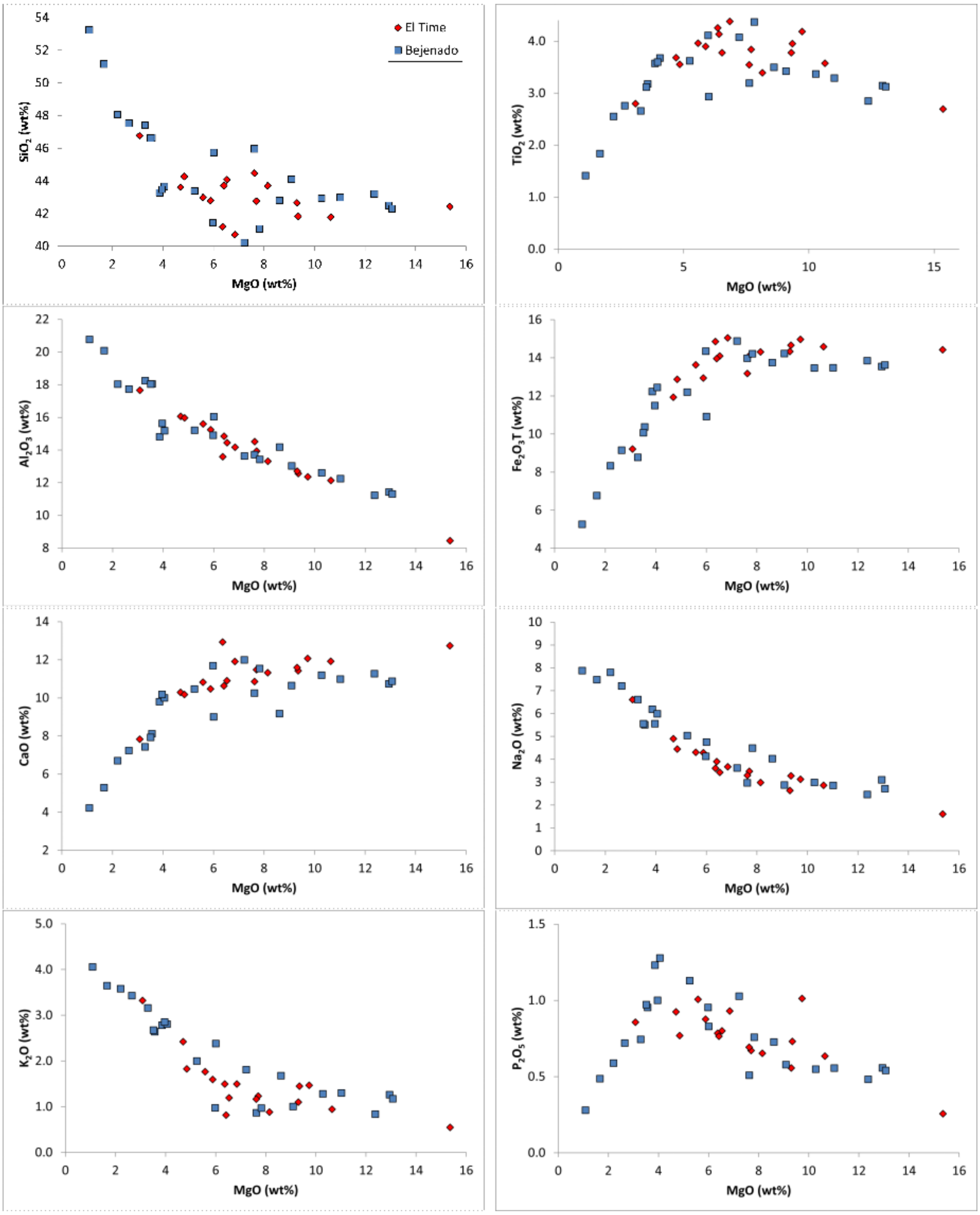

Figure 4A. Major element compositions for pre- and post-collapse lavas from La Palma, plotted against MgO as a function of fractionation. Pre-collapse samples from El Time are shown as red diamonds; post-collapse lavas from Bejenado are shown as blue squares.

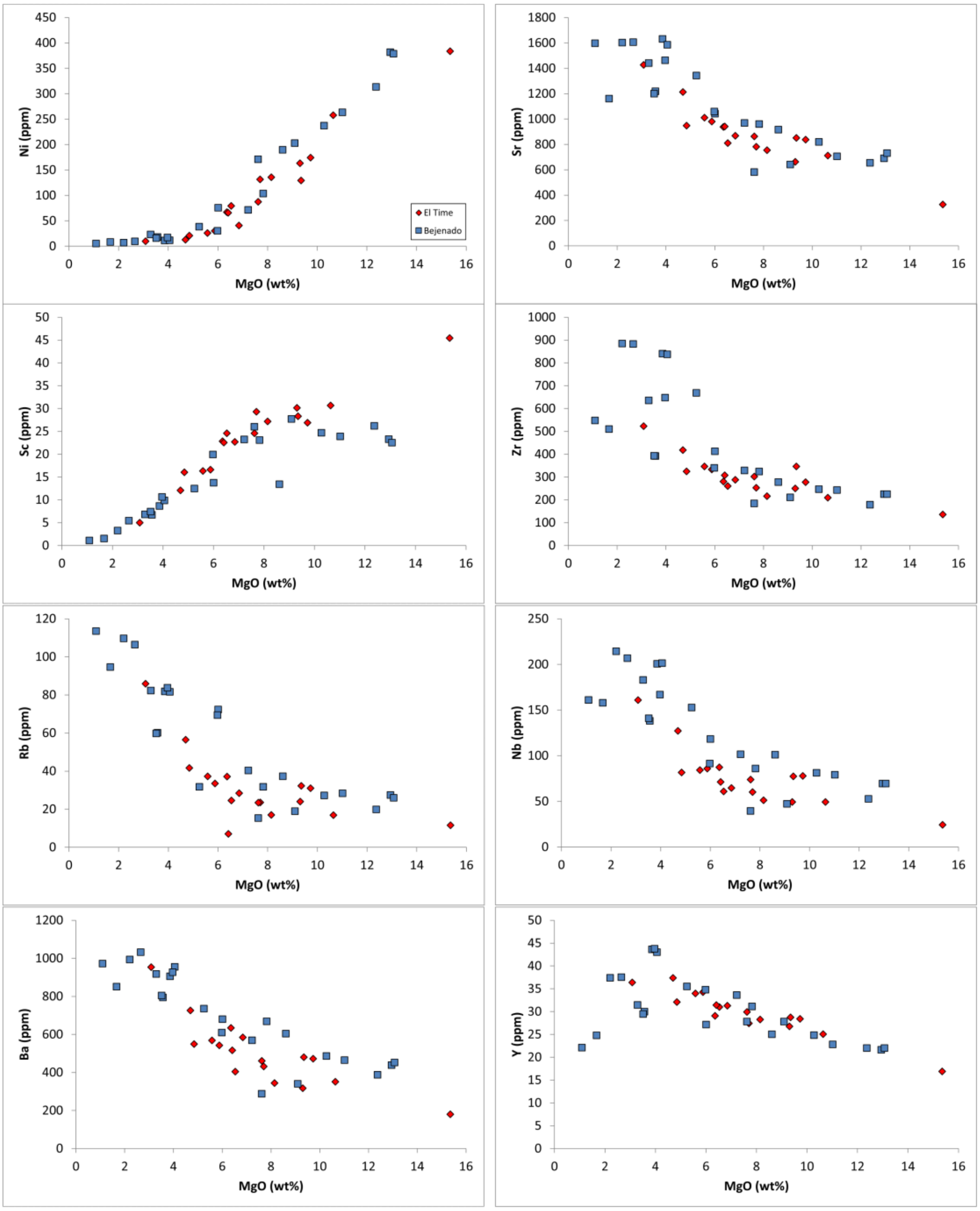

Figure 4B. Selected trace element compositions for pre- and post-collapse lavas from La Palma, vs. MgO. Pre-collapse samples = red diamonds; post-collapse lavas = blue squares.

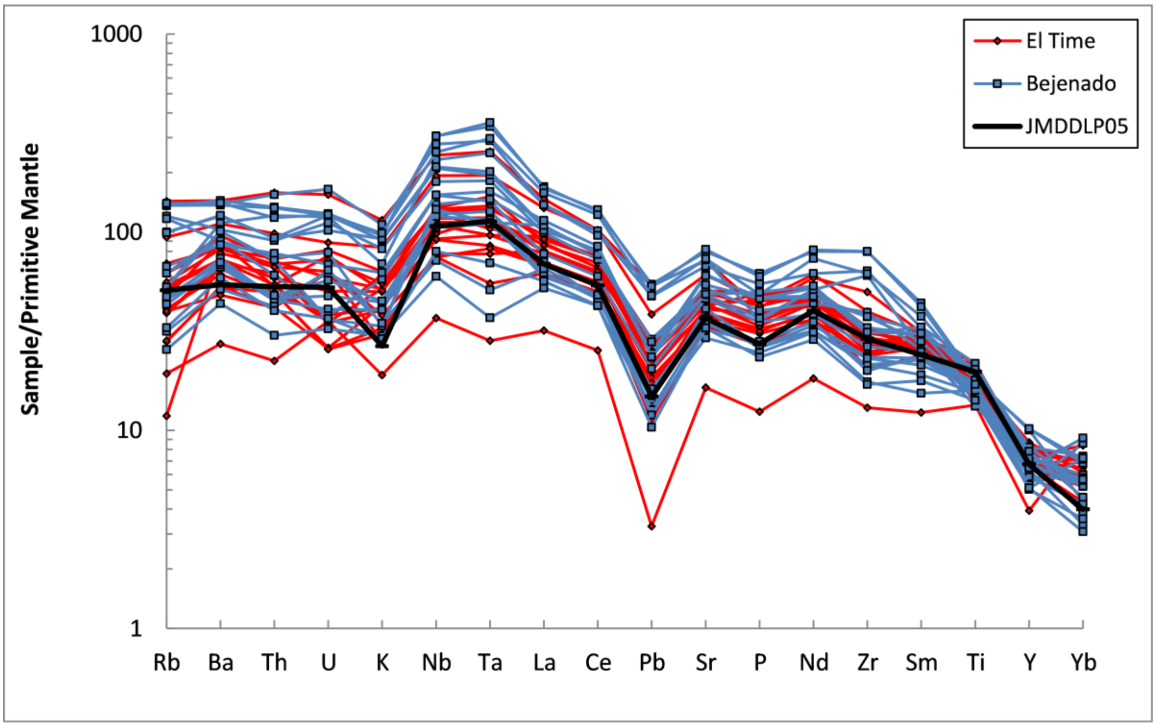

Figure 5. Mantle-normalised trace element diagrams for pre- and post-collapse lavas from La Palma analysed in this study, compared with a sample of pre-collapse lava from Taburiente from Day et al. (2010). Pre-collapse samples from El Time are shown in red; post-collapse lavas from Bejenado are shown in blue.

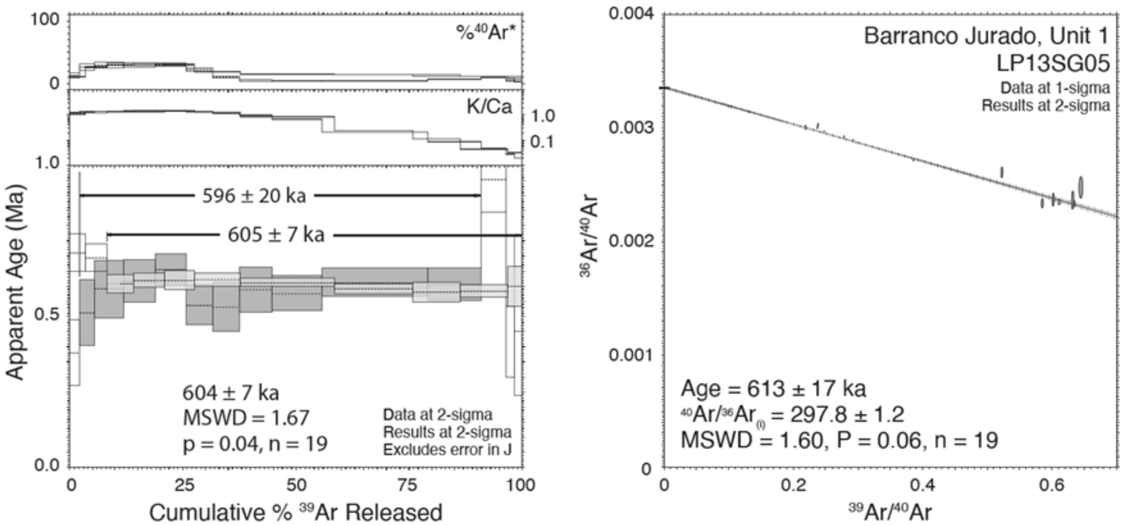

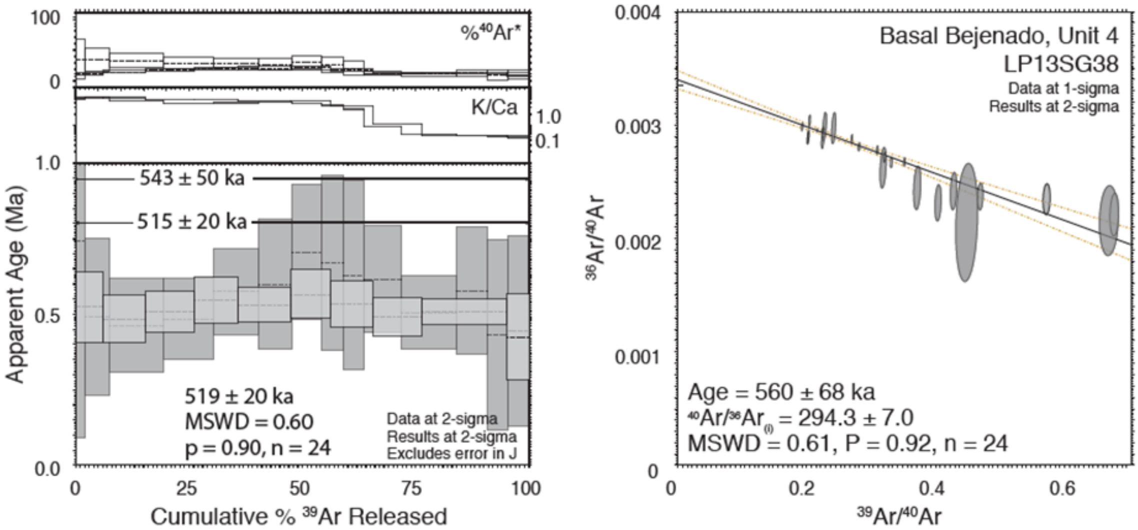
%^{40}Ar*
K/Ca
543 ± 50 ka
515 ± 20 ka
519 ± 20 ka
MSWD = 0.60
p = 0.90, n = 24
Data at 2-sigma
Results at 2-sigma
Excludes error in J
Apparent Age (Ma)
Cumulative % ^{39}Ar Released
Basal Bejenado, Unit 4
LP13SG38
Data at 1-sigma
Results at 2-sigma
Age = 560 ± 68 ka
^{40}Ar/^{36}Ar$_{(i)}$ = 294.3 ± 7.0
MSWD = 0.61, P = 0.92, n = 24
^{36}Ar/^{40}Ar
^{39}Ar/^{40}Ar

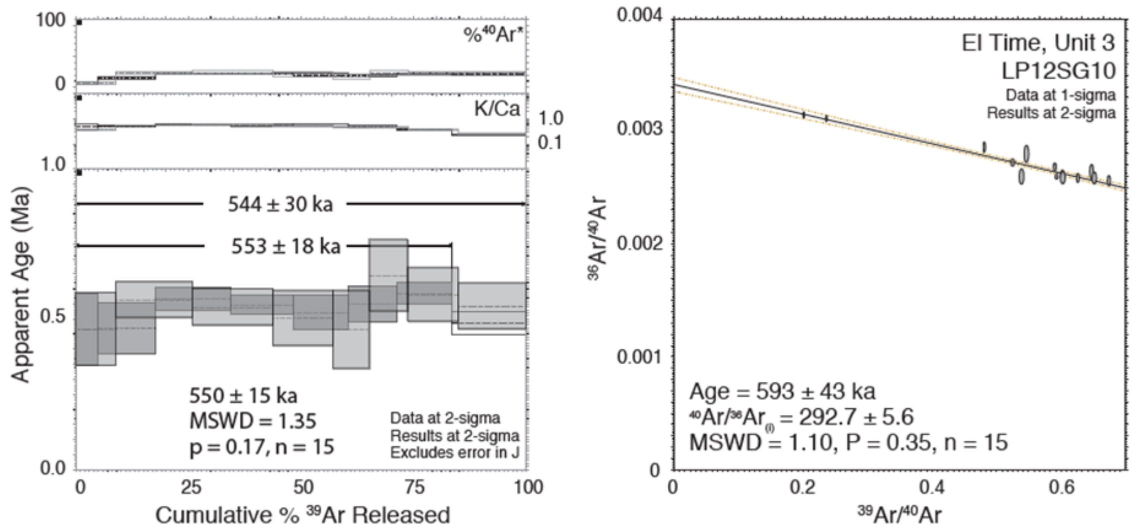
%^{40}Ar*
K/Ca
544 ± 30 ka
553 ± 18 ka
550 ± 15 ka
MSWD = 1.35
p = 0.17, n = 15
Data at 2-sigma
Results at 2-sigma
Excludes error in J
Apparent Age (Ma)
Cumulative % ^{39}Ar Released
El Time, Unit 3
LP12SG10
Data at 1-sigma
Results at 2-sigma
Age = 593 ± 43 ka
^{40}Ar/^{36}Ar$_{(i)}$ = 292.7 ± 5.6
MSWD = 1.10, P = 0.35, n = 15
^{36}Ar/^{40}Ar
^{39}Ar/^{40}Ar

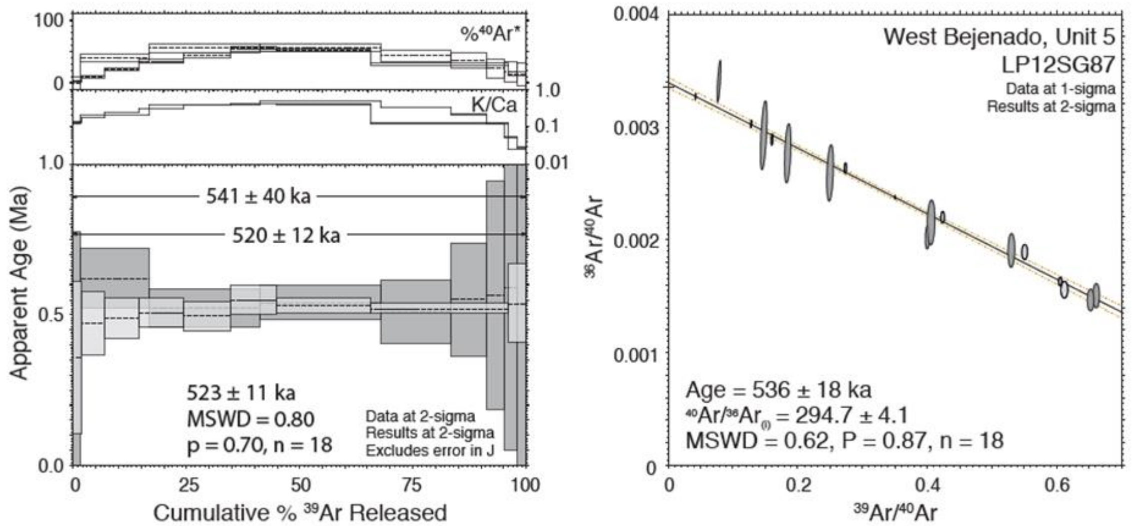
%^{40}Ar*
K/Ca
541 ± 40 ka
520 ± 12 ka
523 ± 11 ka
MSWD = 0.80
p = 0.70, n = 18
Data at 2-sigma
Results at 2-sigma
Excludes error in J
Apparent Age (Ma)
Cumulative % ^{39}Ar Released
West Bejenado, Unit 5
LP12SG87
Data at 1-sigma
Results at 2-sigma
Age = 536 ± 18 ka
^{40}Ar/^{36}Ar$_{(i)}$ = 294.7 ± 4.1
MSWD = 0.62, P = 0.87, n = 18
^{36}Ar/^{40}Ar
^{39}Ar/^{40}Ar

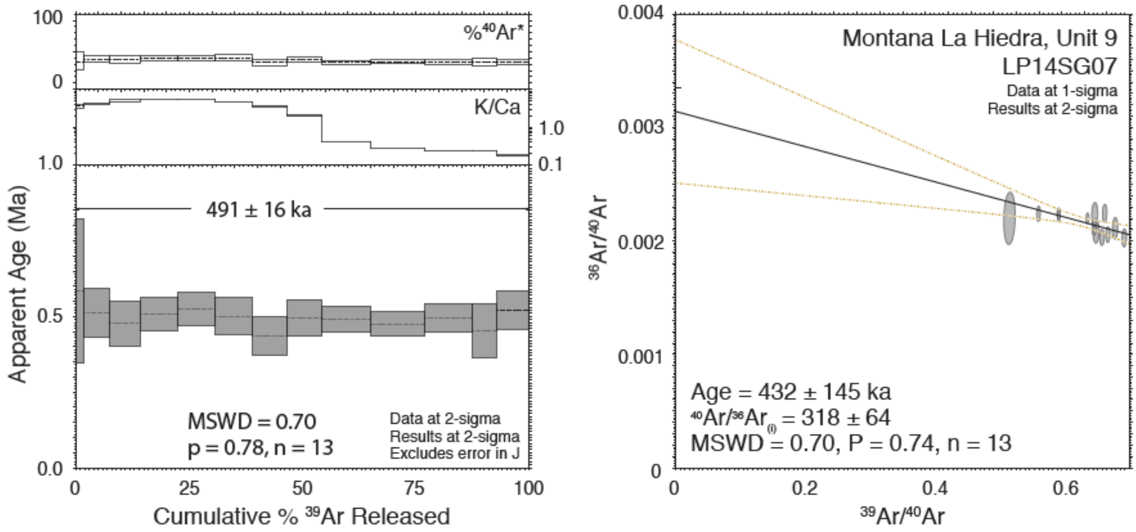

Figure 6. Representative Ar-Ar results for pre- and post-collapse lavas from central La Palma (this study). MSWD: mean square of weighted deviations; p: probability that uncertainties are accounted for by analytical errors alone; n: number of steps comprising the plateau or isochron

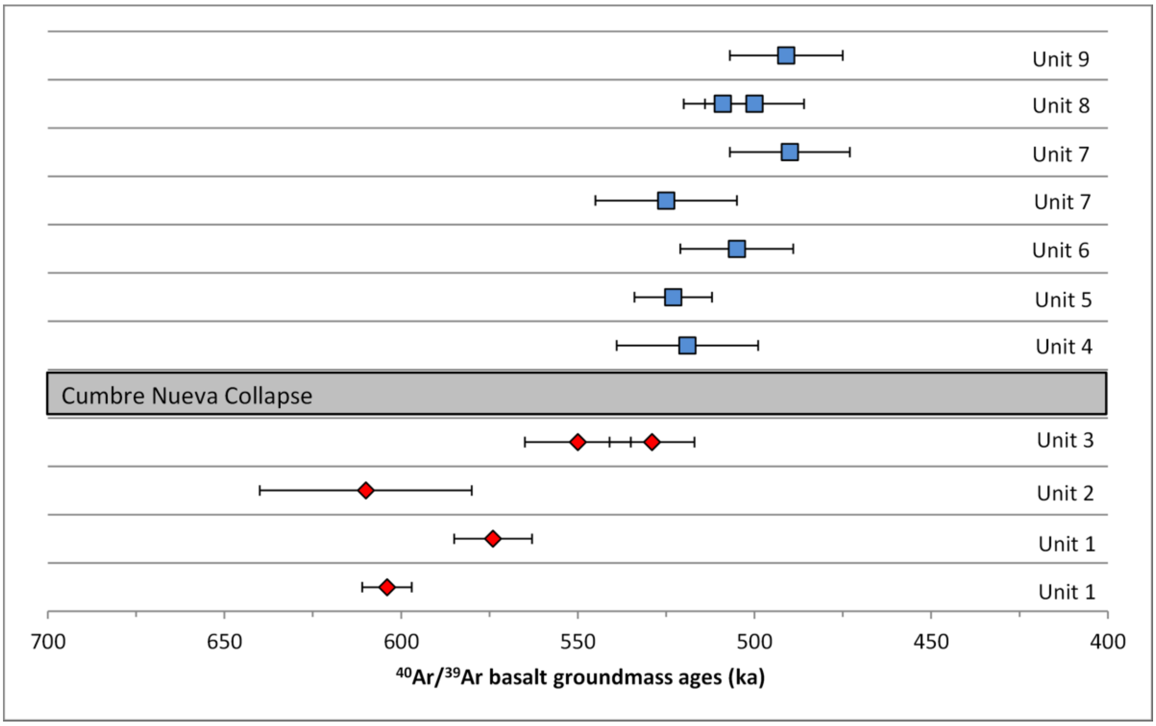

Figure7. $^{40}Ar/^{39}Ar$ age determinations from collapse-related lava flows (this study). Red diamonds = pre-collapse samples; blue squares = post-collapse samples. Errors are 2 sigma standard deviation.

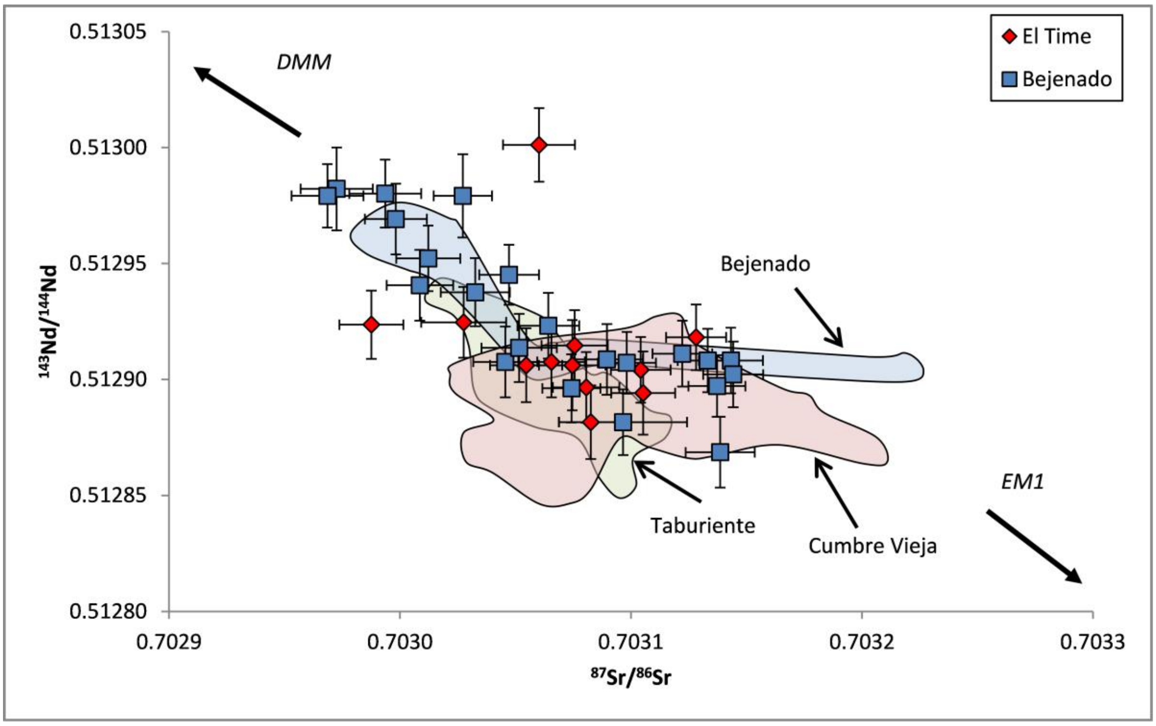

Figure 8. Sr-Nd isotope compositions for pre- and post-collapse lavas from La Palma (this study) compared with literature data (Gallipp, 2005; Praegel and Holm, 2005; Gurenko et al., 2006; Day et al., 2010). Red diamonds = pre-collapse samples from El Time; blue squares = post-collapse samples from Bejenado.

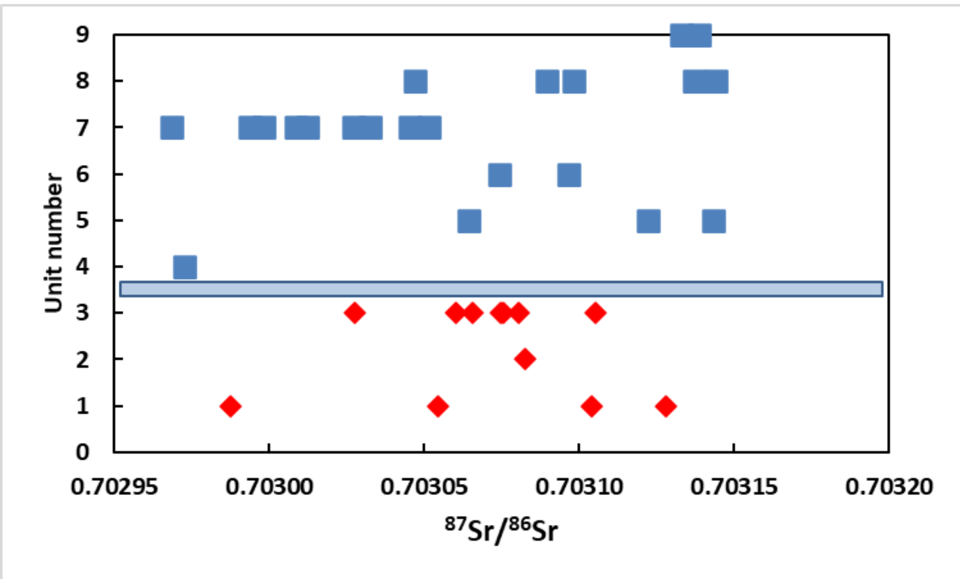

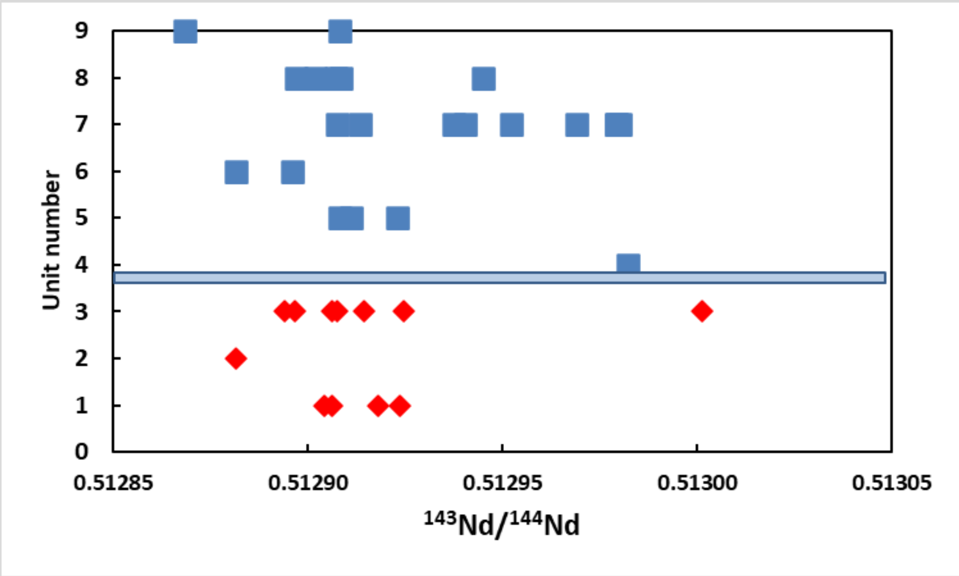
Unit number
0
1
2
3
4
5
6
7
8
9
0.51285
0.51290
0.51295
0.51300
0.51305
$^{143}Nd/^{144}Nd$

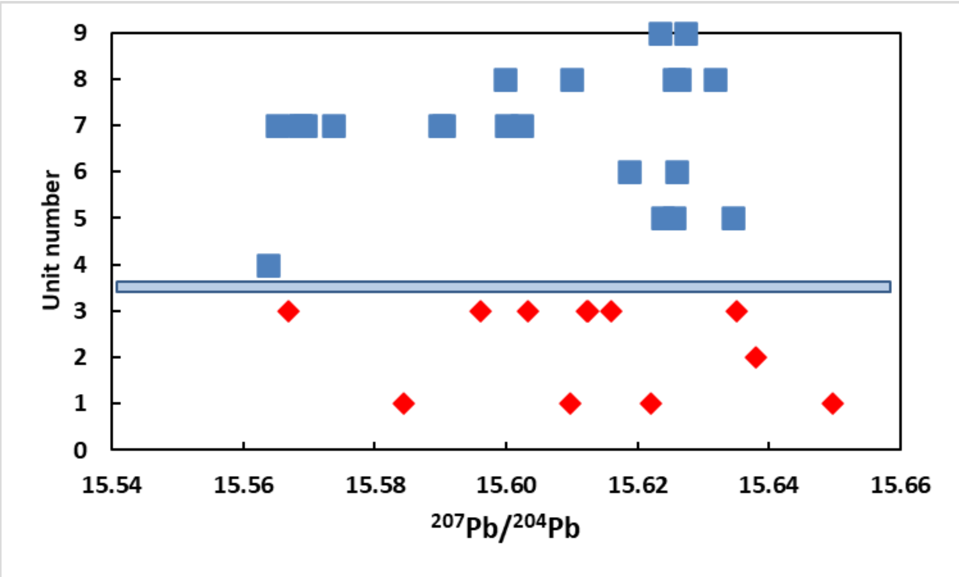
Unit number
0
1
2
3
4
5
6
7
8
9
15.54
15.56
15.58
15.60
15.62
15.64
15.66
$^{207}Pb/^{204}Pb$

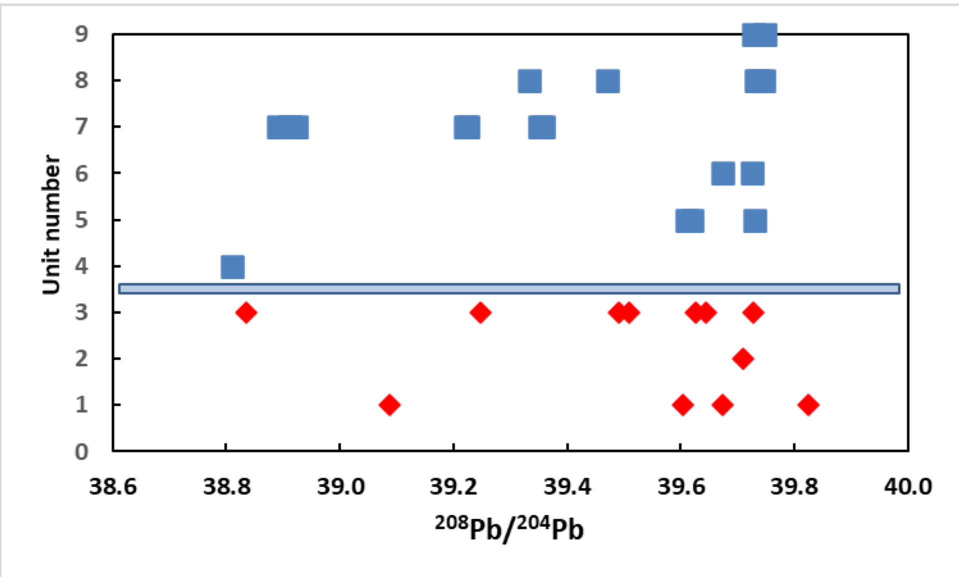
Unit number
0
1
2
3
4
5
6
7
8
9
38.6
38.8
39.0
39.2
39.4
39.6
39.8
40.0
$^{208}Pb/^{204}Pb$

Figure 9. Radiogenic isotope data for pre- and post-collapse lavas from La Palma (this study) in stratigraphic order. Red diamonds = pre-collapse samples from El Time; blue squares = post-collapse samples from Bejenado.

REFERENCES

Blahut, J., Klimeš, J., Rowberry, M. and Kusák, M., 2018. Database of giant landslides on volcanic islands—first results from the Atlantic Ocean. *Landslides*, *15*(4), pp.823-827.

Carracedo, J.C., Day, S., Guillou, H., Badiola, E.R., Canas, J.A. and Torrado, F.P., 1998. Hotspot volcanism close to a passive continental margin: the Canary Islands. *Geological Magazine*, *135*(5), pp.591-604.

Carracedo, J.C., 1999. Growth, structure, instability and collapse of Canarian volcanoes and comparisons with Hawaiian volcanoes. *Journal of Volcanology and Geothermal Research*, *94*(1-4), pp.1-19.

Carracedo, J.C., Day, S.J., Guillou, H. and Torrado, F.J.P., 1999a. Giant Quaternary landslides in the evolution of La Palma and El Hierro, Canary Islands. *Journal of Volcanology and Geothermal Research*, *94*(1-4), pp.169-190.

Carracedo, J.C., Day, S.J., Guillou, H. and Gravestock, P., 1999b. Later stages of volcanic evolution of La Palma, Canary Islands: Rift evolution, giant landslides, and the genesis of the Caldera de Taburiente. *Geological Society of America Bulletin*, *111*(5), pp.755-768.

Carracedo, J.C., Rodriguez-Badiola, E., Guillou, H., Nuez Pestana, J.D.L. and Pérez Torrado, F.J., 2001. Geology and volcanology of la Palma and el Hierro, western Canaries. *Estudios Geológicos* 57, 175-273

Carracedo, J.C., Badiola, E.R., Guillou, H., Paterne, M., Scaillet, S., Torrado, F.P., Paris, R., Fra-Paleo, U. and Hansen, A., 2007. Eruptive and structural history of Teide Volcano and rift zones of Tenerife, Canary Islands. *Geological Society of America Bulletin*, *119*(9-10), pp.1027-1051.

Colmenero, J.R., De la Nuez, J., Casillas, R. and Castillo, C., 2012. Epiclastic deposits associated with large-scale landslides and the formation of erosive calderas in oceanic islands: The example of the La Palma Island (CanaryArchipelago). *Geomorphology*, *177*, pp.108-127.

Cornu, M.N., Paris, R., Doucelance, R., Bachèlery, P., Bosq, C., Auclair, D., Benbakkar, M., Gannoun, A.M. and Guillou, H., 2021. Exploring the links between volcano flank collapse and the magmatic evolution of an ocean island volcano: Fogo, Cape Verde. *Scientific Reports*, *11*(1), pp.1-12.

Day, S.J., Da Silva, S.H. and Fonseca, J.F.B.D., 1999. A past giant lateral collapse and present-day flank instability of Fogo, Cape Verde Islands. *Journal of Volcanology and Geothermal Research*, *94*(1-4), pp.191-218.

Day, J.M., Pearson, D.G., Macpherson, C.G., Lowry, D. and Carracedo, J.C., 2010. Evidence for distinct proportions of subducted oceanic crust and lithosphere in HIMU-type mantle beneath El Hierro and La Palma, Canary Islands. *Geochimica et Cosmochimica Acta*, *74*(22), pp.6565-6589.

Deniel, C. and Pin, C., 2001. Single-stage method for the simultaneous isolation of lead and strontium from silicate samples for isotopic measurements. *Analytica Chimica Acta*, *426*(1), pp.95-103.

Foeken, J.P., Day, S. and Stuart, F.M., 2009. Cosmogenic ^{3}He exposure dating of the Quaternary basalts from Fogo, Cape Verdes: implications for rift zone and magmatic reorganisation. *Quaternary Geochronology*, *4*(1), pp.37-49.

Galipp, K., 2005. *Geochemical and petrological evolution of La Palma (Canary Islands) and its rift zone during the last 1.0 Ma* (Doctoral dissertation, Universität Bremen).

Guillou, H., Carracedo, J.C. and Day, S.J., 1998. Dating of the upper Pleistocene–Holocene volcanic activity of La Palma using the unspiked K–Ar technique. *Journal of Volcanology and Geothermal Research*, *86*(1-4), pp.137-149.

Guillou, H., Carracedo, J.C. and Duncan, R.A., 2001. K–Ar, ^{40}Ar–^{39}Ar ages and magnetostratigraphy of Brunhes and Matuyama lava sequences from La Palma Island. *Journal of Volcanology and Geothermal Research*, *106*(3-4), pp.175-194.

Guillou, H., Torrado, F.J.P., Machin, A.R.H., Carracedo, J.C. and Gimeno, D., 2004a. The Plio–Quaternary volcanic evolution of Gran Canaria based on new K–Ar ages and magnetostratigraphy. *Journal of Volcanology and Geothermal Research*, *135*(3), pp.221-246.

Guillou, H., Carracedo, J.C., Paris, R. and Torrado, F.J.P., 2004b. Implications for the early shield-stage evolution of Tenerife from K/Ar ages and magnetic stratigraphy. *Earth and Planetary Science Letters*, *222*(2), pp.599-614.

Gurenko, A.A., Hoernle, K.A., Hauff, F., Schmincke, H.U., Han, D., Miura, Y.N. and Kaneoka, I., 2006. Major, trace element and Nd–Sr–Pb–O–He–Ar isotope signatures of shield stage lavas from the central and western Canary Islands: insights into mantle and crustal processes. *Chemical Geology*, *233*(1-2), pp.75-112.

Hunt, J.E. and Jarvis, I., 2017. Prodigious submarine landslides during the inception and early growth of volcanic islands. *Nature communications*, *8*(1), p.2061.

Hunt, J.E., Wynn, R.B., Talling, P.J. and Masson, D.G., 2013. Multistage collapse of eight western Canary Island landslides in the last 1.5 Ma: Sedimentological and geochemical evidence from subunits in submarine flow deposits. *Geochemistry, Geophysics, Geosystems*, *14*(7), pp.2159-2181.

Hürlimann, M., Martí, J. and Ledesma, A., 2004. Morphological and geological aspects related to large slope failures on oceanic islands: The huge La Orotava landslides on Tenerife, Canary Islands. *Geomorphology*, *62*(3-4), pp.143-158.

Krastel, S., Schmincke, H.U., Jacobs, C.L., Rihm, R., Le Bas, T.P. and Alibes, B., 2001. Submarine landslides around the Canary Islands. *Journal of Geophysical Research: Solid Earth*, *106*(B3), pp.3977-3997.

León, R., Somoza, L., Urgeles, R., Medialdea, T., Ferrer, M., Biain, A., García-Crespo, J., Mediato, J.F., Galindo, I., Yepes, J. and González, F.J., 2017. Multi-event oceanic island landslides: New onshore-offshore insights from El Hierro Island, Canary Archipelago. *Marine Geology*, *393*, pp.156-175.

Longpré, M.A., Chadwick, J.P., Wijbrans, J. and Iping, R., 2011. Age of the El Golfo debris avalanche, El Hierro (Canary Islands): New constraints from laser and furnace $^{40}Ar/^{39}Ar$ dating. *Journal of Volcanology and Geothermal research*, *203*(1-2), pp.76-80.

Mark, D.F., Barfod, D., Stuart, F.M. and Imlach, J., 2009. The ARGUS multicollector noble gas mass spectrometer: Performance for $^{40}Ar/^{39}Ar$ geochronology. *Geochemistry, Geophysics, Geosystems*, *10*(10).

Martí, J., Hurlimann, M., Ablay, G.J. and Gudmundsson, A., 1997. Vertical and lateral collapses on Tenerife (Canary Islands) and other volcanic ocean islands. *Geology*, *25*(10), pp.879-882.

Masson, D.G., 1996. Catastrophic collapse of the volcanic island of Hierro 15 ka ago and the history of landslides in the Canary Islands. *Geology*, *24*(3), pp.231-234.

Masson, D.G., Watts, A.B., Gee, M.J.R., Urgeles, R., Mitchell, N.C., Le Bas, T.P. and Canals, M., 2002. Slope failures on the flanks of the western Canary Islands. *Earth-Science Reviews*, *57*(1-2), pp.1-35.

Moore, J.G., Clague, D.A., Holcomb, R.T., Lipman, P.W., Normark, W.R. and Torresan, M.E., 1989. Prodigious submarine landslides on the Hawaiian Ridge. *Journal of Geophysical Research: Solid Earth*, *94*(B12), pp.17465-17484.

Navarro, J.M. and Coello, J., 1994. Mapa geológico del PN Taburiente. *ICONA (in Spanish)*.

Niespolo E.M., Rutte D., Deino A.L., Renne P. R. 2017. Intercalibration and age of the Alder Creek sanidine Ar-40/Ar-39 standard. *Quaternary Geochronology* 39, 205-213. 10.1016/j.quageo.2016.09.004

Paris, R. and Carracedo, J.C., 2001. Formation d'une caldera d'érosion et instabilité récurrente d'une île de point chaud: la caldera de Taburiente, La Palma, îles

Canaries/Formation of an erosion caldera and recurring instability on a hotspot-generated island: the caldera de Taburiente, La Palma, Canary Islands. *Géomorphologie: relief, processus, environnement*, *7*(2), pp.93-105.

Prægel, N.O. and Holm, P.M., 2006. Lithospheric contributions to high-MgO basanites from the Cumbre Vieja Volcano, La Palma, Canary Islands and evidence for temporal variation in plume influence. *Journal of Volcanology and Geothermal Research*, *149*(3-4), pp.213-239.

Renne, P R., Balco G, Ludwig K R, Mundil R, and Min K 2011. "Response to the comment by WH Schwarz et al. on “Joint determination of ^{40}K decay constants and ^{40}Ar∗/^{40}K for the Fish Canyon sanidine standard, and improved accuracy for ^{40}Ar/^{39}Ar geochronology” by Renne P.R. et al. (2010)." *Geochimica et Cosmochimica Acta* 75, no. 17: 5097-5100.

Sparks, R.S.J., Folkes, C.B., Humphreys, M.C., Barfod, D.N., Clavero, J., Sunagua, M.C., McNutt, S.R. and Pritchard, M.E., 2008. Uturuncu volcano, Bolivia: Volcanic unrest due to mid-crustal magma intrusion. *American Journal of Science*, *308*(6), pp.727-769.

Staudigel, H. and Schmincke, H.U., 1984. The Pliocene seamount series of La Palma Canary Islands. *Journal of Geophysical Research: Solid Earth*, *89*(B13), pp.11195-11215.

Thirlwall, M.F., 2002. Multicollector ICP-MS analysis of Pb isotopes using a ^{207}Pb-^{204}Pb double spike demonstrates up to 400 ppm/amu systematic errors in Tl normalization. *Chemical Geology*, *184*(3-4), pp.255-279.

Thirlwall, M.F., Singer, B.S. and Marriner, G.F., 2000. ^{39}Ar–^{40}Ar ages and geochemistry of the basaltic shield stage of Tenerife, Canary Islands, Spain. *Journal of Volcanology and Geothermal Research*, *103*(1-4), pp.247-297.

van den Bogaard, P., 2013. The origin of the Canary Island Seamount Province-New ages of old seamounts. *Scientific Reports*, *3*(1), pp.1-7.

Watt, S.F., 2019. The evolution of volcanic systems following sector collapse. *Journal of Volcanology and Geothermal Research*, *384*, pp.280-303.